Multiscale Four-Dimensional Data Assimilation

DAVID R. STAUFFER AND NELSON L. SEAMAN

The Pennsylvania State University, University Park, Pennsylvania

(Manuscript received 22 December 1992, in final form 3 September 1993)

ABSTRACT

Four-dimensional data assimilation (FDDA) schemes capable of effectively analyzing asynoptic, near-continuous data streams are especially important on the mesobeta scale for both model initialization and dynamic analysis. A multiscale nudging approach that utilizes grid nesting is investigated for the generation of complete, dynamically consistent datasets for the mesobeta scale. These datasets are suitable for input into air quality models, but can also be used for other diagnostic purposes including model initialization. A multiscale nudging strategy is used here to simulate the wind flow for two cases over the Colorado Plateau and Grand Canyon region during the winter of 1990 when a special mesobeta-scale observing system was deployed in the region to study the canyon's visibility impairment problem. The special data included Doppler sodars, profilers, rawinsondes, and surface stations. Combinations of these data and conventional mesoalpha-scale data were assimilated into a nested version of the Pennsylvania State University–National Center for Atmospheric Research Mesoscale Model to investigate the importance of scale interaction and scale separation during FDDA.

Mesoalpha-scale forcing was shown to be important for accurate simulation of the mesobeta-scale flow over the 48-h period of the simulations. Direct assimilation of mesoalpha-scale analyses on a finescale grid was shown to be potentially harmful to the simulation of mesobeta-scale features. Nudging to mesoalpha-scale analyses on the coarse grid enabled nudging to mesobeta-scale observations on the inner fine grid to be more effective. This grid-nesting, multiscale FDDA strategy produced the most accurate simulation of the low-level wind fields. It is demonstrated that when designing an FDDA strategy, scale interactions of different flow regimes cannot be ignored, particularly for simulation periods of several days on the mesobeta scale.

1. Introduction

The rapid growth and availability of economical computer power, in terms of larger memory, higher speed, and massive parallelization, has led to correspondingly finer resolution numerical weather prediction models in the hope of improving our understanding and our ability to simulate complex atmospheric processes. However, it has become increasingly clear that greater resolution alone cannot ensure equally great gains in model skill. At least two additional factors are crucial for improving current numerical models: better use of available data on the atmospheric state and better representation of physical processes such as convection, turbulence, and radiation.

This paper addresses the issue of data use, which will become especially urgent in the 1990s as remote sensing instrumentation is deployed more or less routinely to gather atmospheric measurements both operationally and in high-resolution research arrays. These instruments, such as profilers, sodars, lidars, NEXRAD (Next Generation Weather Radar) Doppler radars, ASOS (Automatic Surface Observing System), improved satellite sounding systems, and ACARS (Automated Commercial Aircraft Reporting System), are providing a rapidly expanding near-continuous stream of data on evolving atmospheric conditions. The near-continuous data streams and growing computer power are now making mesobeta-scale numerical modeling of real-data cases increasingly practical. Continuous four-dimensional data assimilation (FDDA) schemes capable of effectively analyzing this database are a vital component in what may prove to be a new numerical modeling revolution by 1) improving the initialization of mesoscale forecasts and 2) generating high-quality four-dimensional mesoscale analyses for diagnostic purposes and input into advanced Eulerian photochemical and air quality models (Stauffer et al. 1993).

At synoptic and mesoalpha scales, FDDA has already been applied successfully for both of these purposes. For example, Bell (1986) described an FDDA scheme used to initialize an operational limited-area forecast model at the United Kingdom Meteorological Office (UKMO). Seaman (1992) used a similar technique to generate the meteorological input to an Eulerian acid-deposition model applied to the eastern United States. In both of these examples, the technique of Newtonian relaxation, or "nudging," described by Stauffer and Seaman (1987, 1990) and Stauffer et al. (1991), was found to be an effective and economical method for performing FDDA.

Corresponding author address: Dr. David R. Stauffer, Department of Meteorology, The Pennsylvania State University, 503 Walker Building, University Park, PA 16802.

A typical example of data collection and numerical modeling at the *mesobeta scale* is found in the growing number of studies intended to help decision makers implement the 1990 Clean Air Act. In the design of several of the current regional air quality programs, mesobeta-scale numerical weather prediction and FDDA techniques are expected to play a significant role. There are, however, significant problems associated with modeling applications for real-data cases of more than 24 h on the mesobeta scale. Economic constraints generally prevent the remote sensing systems from being distributed uniformly over even a very limited domain of interest. Thus, the distribution of the data available for analysis, FDDA, and model evaluation is often highly nonuniform. Additional problems include the rapid evolution of mesobeta-scale flows, their sensitivity to major "decision" events (such as the onset of deep convection), and incomplete observations (e.g., profilers provide good wind data but at present are not widely used to provide mass field information). These factors make it uncertain whether FDDA techniques applied to a limited database can be successful for periods of several days or more at these finer scales or, if so, under what conditions?

As a beginning toward understanding the conditions under which continuous FDDA might be an effective tool for improving the simulation of *mesobeta-scale* events with high-resolution limited-area models, this investigation considers a *multiscale* nudging strategy to simulate *wind flow* in two real wintertime cases over the Colorado Plateau and Grand Canyon region, with emphasis on the period of 18–20 January 1990. In the winter of 1990, a special mesobeta-scale observing system was deployed in the Grand Canyon region, under the sponsorship of Salt River Project, to study the canyon's widely publicized visibility impairment problem. The special data included Doppler sodars, profilers, rawinsondes, and surface stations. Combinations of these data and conventional data are assimilated into a nested version of the Pennsylvania State University–National Center for Atmospheric Research (PSU–NCAR) Mesoscale Model to investigate the importance of scale interaction and scale separation during FDDA.

The main objective of this study is to determine an effective multiscale approach by which FDDA can be used to better simulate mesobeta-scale flows using a nested-grid model with a 30-km coarse domain and a 10-km fine domain. To this end FDDA experiments are performed that rely on 1) assimilation of only conventional mesoalpha-scale analyses on the coarse grid to improve the time-continuous lateral boundary conditions supplied to the inner fine grid, 2) direct assimilation of only asynoptic mesobeta-scale observations within the fine domain, and 3) combinations of these two approaches that include direct assimilation of mesoalpha-scale analyses on the fine domain. Another objective of the study is to determine under what conditions FDDA can be potentially harmful to the simulation of mesobeta-scale features.

The following section describes the modeling system used in this study, followed by a review of the general nudging strategy and the technique used to assimilate the special asynoptic dataset. The experimental design is described in section 3, and a review of the case study follows in section 4. The results are presented in section 5 and summarized in section 6.

2. Description of the mesoscale modeling system

a. The PSU–NCAR model

The assimilating model is the three-dimensional hydrostatic version of the PSU–NCAR model described by Anthes et al. (1987) and written in the terrain-following sigma (nondimensionalized pressure) coordinate. In this application, a multilayer Blackadar parameterization scheme is used to represent planetary boundary layer (PBL) processes, including surface fluxes of heat, moisture, and momentum (Zhang and Anthes 1982). Ground temperature is predicted with a surface energy budget equation, which includes longwave and shortwave irradiances and is dependent on cloud cover, atmospheric pathlength, vapor content, and surface properties, including snow cover.

The model is configured as a two-way-interactive nested-grid system (Zhang et al. 1986), in which both the coarse-grid mesh (CGM, Δx = 30 km) and fine-grid mesh (FGM, Δx = 10 km) have 61 × 61 points (Fig. 1). The lateral boundaries of the coarse grid are specified from observations by temporally interpolating 12-h mesoalpha-scale analyses based on standard surface and rawinsonde data. This lateral boundary information is introduced into the model using a relaxation technique. Both domains use 20 layers in the vertical direction, with the model top at p_t = 150 mb. The fine-grid domain is centered near Page, Arizona, close to the Navaho Generating Station (NGS) power plant. Figure 2 shows the local geography and the 10-km terrain surrounding the Grand Canyon; much of the canyon itself is, of course, unresolved at this resolution.

b. The Newtonian relaxation FDDA technique

Newtonian relaxation, or *nudging,* is a continuous data assimilation method that relaxes the model state toward the observed state by adding to one or more of the prognostic equations artificial tendency terms based on the difference between the two states. In this application, the two approaches described in Stauffer and Seaman (1990) and Stauffer et al. (1991) are used: 1) nudging toward gridded analyses based on synoptic observations and interpolated to the model's current time step, and 2) nudging directly toward individual observations distributed nonuniformly in space and

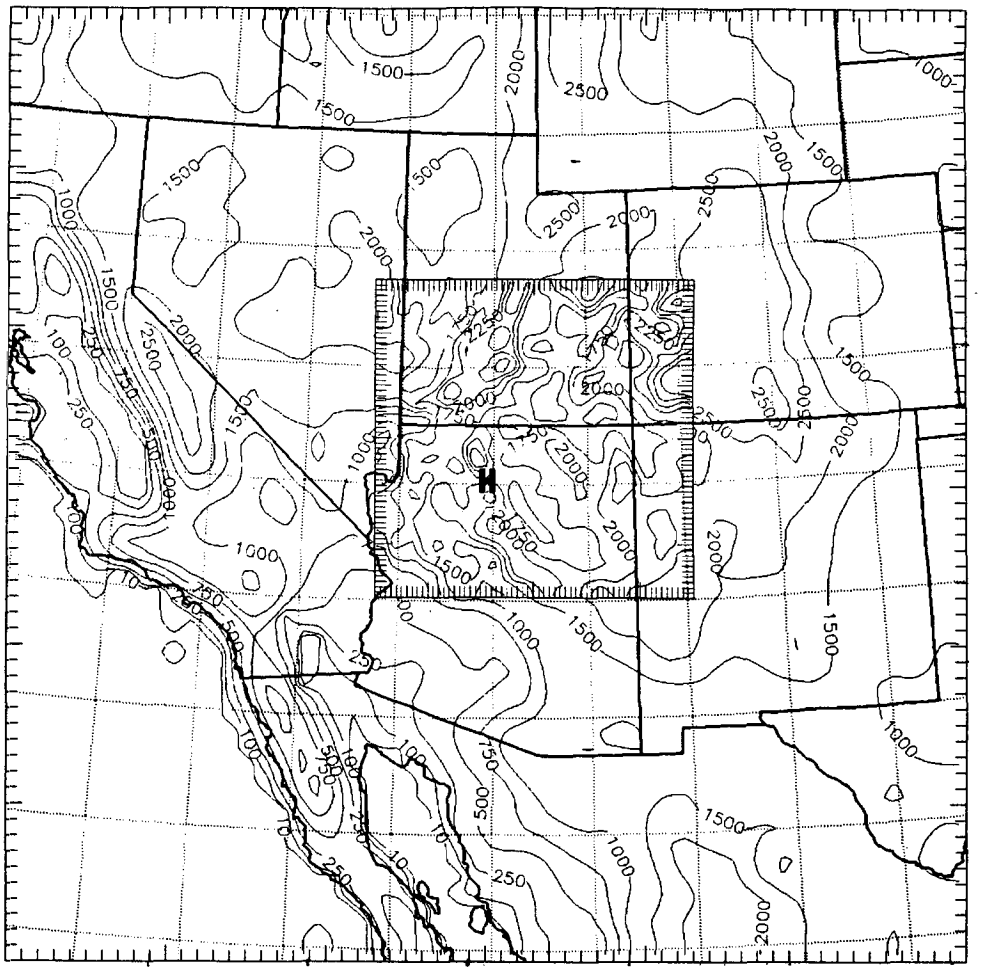

FIG. 1. Mesoscale model domains and terrain (m). On the coarse-grid mesh (Δx = 30 km, outer box), the contour interval is 250 m below an elevation of 1000 m and 500 m above 1000 m. The contour interval on the fine-grid mesh (Δx = 10 km, inner box) is 250 m; *H* denotes Hopi Point, Arizona (Grand Canyon).

time. These two approaches are hereafter referred to as "analysis nudging" and "obs nudging," respectively.

As discussed in Stauffer and Seaman (1990), when pressure is not assimilated the general form of the predictive equation for variable $\alpha(\mathbf{x}, t)$ is written in flux form (i.e., $p*\alpha$, where $p^* = p_s - p_t$, and p_s is surface pressure, and p_t is a constant pressure at the top of the model) as

$$\frac{\partial p*\alpha}{\partial t} = F(\alpha, \mathbf{x}, t) + G_\alpha W(\mathbf{x}, t)\epsilon(x)p*(\hat{\alpha}_0 - \alpha). \quad (1)$$

All of the model's physical forcing terms are represented by F where α are the model's dependent variables, $\mathbf{x}$ are the independent spatial variables, and t is time. The second term on the right side of (1) represents the analysis nudging term for α. The estimate of the observation analyzed to the grid and interpolated linearly in time to t is $\hat{\alpha}_0$. Confidence in the analysis is specified by ϵ, the analysis quality factor, which ranges between 0 and 1 and is based on the quality and distribution of the data used to produce the gridded analysis. The nudging factor G_α determines the relative magnitude of the term, while W specifies the horizontal, vertical, and time weighting applied to the analysis where $W = w_{xy}w_\sigma w_t$.

The second approach, "obs nudging," does not require gridded analyses of the observations and is better suited for assimilation of high-frequency asynoptic data (e.g., profilers). Its form is similar to (1) and it uses only those observations that fall within a predetermined time window centered about the current model time step. The set of differences between the model and the observed state is computed at the observation locations. These "corrections" are then analyzed back to the grid

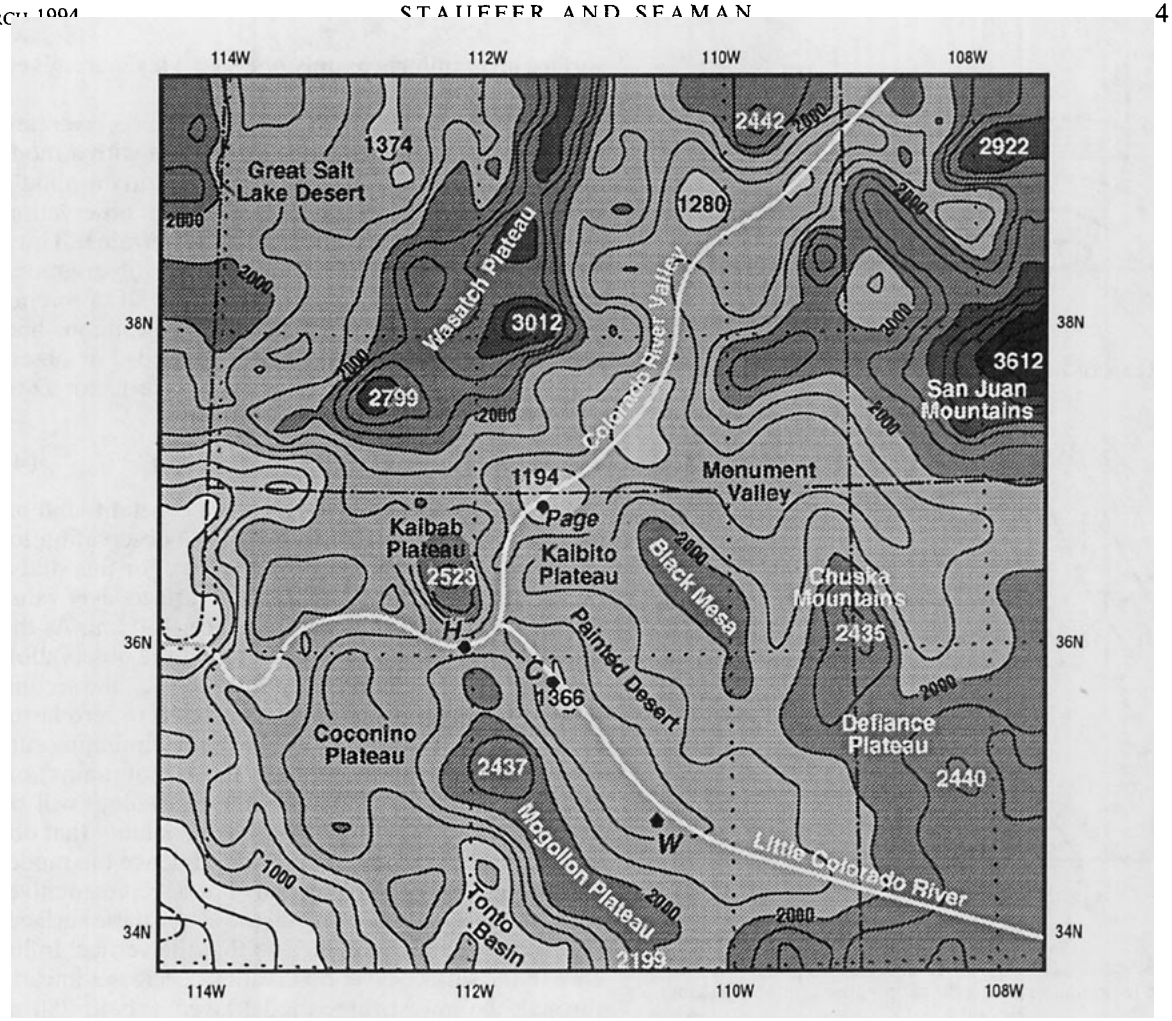

FIG. 2. Fine-grid mesh (Δx = 10 km) terrain (m) and geography, including Grand Canyon and its surroundings: H denotes Hopi Point, Arizona; C is Cameron, Arizona; and W is Winslow, Arizona.

within a region surrounding the observations. The tendency for $\alpha(\mathbf{x}, t)$ is then given by

$$\frac{\partial p^* \alpha}{\partial t} = F(\alpha, \mathbf{x}, t) + G_\alpha p^* \frac{\left[\sum_{i=1}^{N} W_i^2(\mathbf{x}, t)\gamma_i(\alpha_0 - \hat{\alpha})_i\right]}{\sum_{i=1}^{N} W_i(\mathbf{x}, t)}, \quad (2)$$

where F and G_α are as defined earlier, subscript i denotes the ith observation of a total of N that are within a preset radius of a given grid point in both the horizontal and vertical directions, α_0 is the locally observed value of α, and $\hat{\alpha}$ is the model's prognostic variable interpolated to the observation location in three dimensions. The observational quality factor γ, which ranges from 0 to 1, accounts for characteristic errors in measurement systems and representativeness. The four-dimensional weighting function W accounts for the spatial and temporal separation of the ith observation from a given grid point and time step.

For economy, the multilevel observations (soundings) used for obs nudging in this study were vertically interpolated to the model sigma surfaces at each observation location prior to each simulation. Figure 3 illustrates schematically the horizontal and temporal components of W used for nudging to observations. The horizontal weighting function w_{xy} is a Cressman function given by

$$w_{xy} = \begin{cases} \dfrac{R^2 - D^2}{R^2 + D^2}, & D \leq R \\ 0, & D > R \end{cases} \quad (3)$$

(Stauffer and Seaman 1990), where D is the distance from the ith observation location to the grid point and R is the horizontal radius of influence. As shown in the top of Fig. 3, R varies linearly in the vertical with pressure and approaches a preset value R' at a pressure

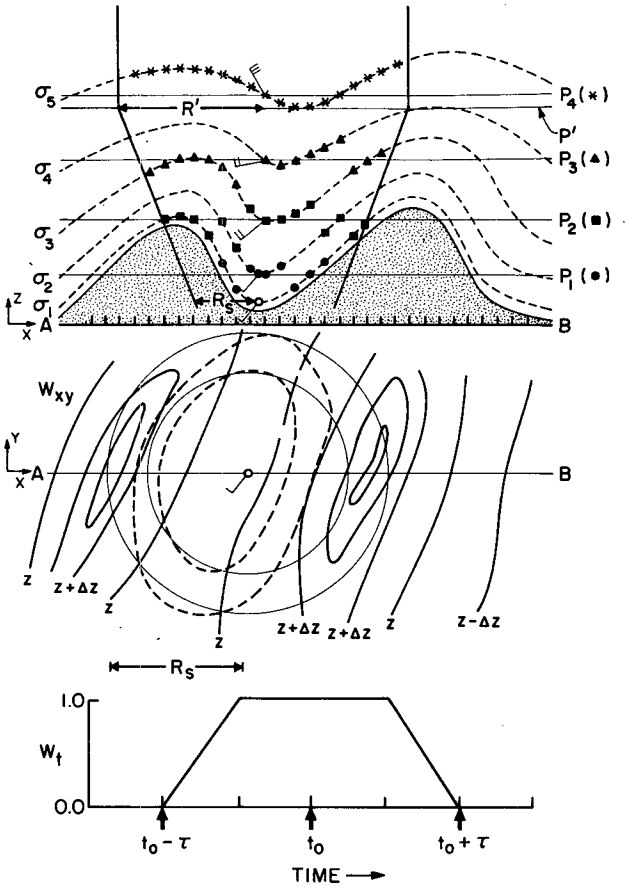

FIG. 3. Schematic showing the horizontal weighting function w_{xy} and the temporal weighting function w_t used for obs nudging.

level p' representing the free atmosphere, where terrain influences are assumed to be small. At pressures less than or equal to this value, defined here as 500 mb, the horizontal radius of influence is defined as twice the value used in the surface layer R_s. For this study, R_s = 100 km and R' = 200 km. For certain situations, such as upward-propagating mountain-induced gravity waves, the assumption of negligible terrain influence within the troposphere is invalid and should be avoided.

As shown in the top of the figure, the corrections computed at a given observation site and vertical level above the surface layer (lowest model layer) are spread laterally along a constant pressure level and thus across several sigma layers in regions of sloping terrain. That is, for any given grid point within the horizontal radius of influence, the obs-nudging correction is in the horizontal direction at the sigma layer that has a pressure value closest to that of the observation. Although the vertical component of the weighting function, w_σ (not shown), is also a distance-weighted function (Stauffer and Seaman 1990), the vertical radius of influence R_σ is defined here to be small (less than the spacing of the model layers) so that each observation above the model surface layer influences only one sigma layer at a given horizontal grid point.

Observations within the model surface layer are spread along constant sigma surfaces but with a modified Cressman function (dashed contours in the middle of Fig. 3) that reduces the influence of an observation as a function of the surface pressure (terrain). Thus, spreading the influence of surface-layer observations along the lowest sigma ensures that the FDDA forcing near the surface in uneven terrain is continuous and not like a pebble skipping across a pond. For observations in the surface layer, the distance factor D in (3) is replaced with D_m,

$$D_m = D + R_s C_m^{-1} \, | p_{so} - p_s |, \qquad (4)$$

where D is as defined above, C_m is a constant, and p_{so} and p_s are the surface pressures at the observation location and the grid point, respectively. For this study, C_m is defined as 75 mb and R_s is the surface-layer value for the horizontal radius of influence, 100 km. As the difference in surface pressure between the observation location and the grid point approaches C_m, the second term in (4) approaches R, and w_{xy} tends to zero faster for a given D. Therefore, the effect of assimilating surface-layer observations in the valley (mountains) on gridpoint locations in the mountains (valley) will be much reduced. This minimizes the possibility that observations in complex terrain will influence the model solution in areas where they may not be representative. Also, the vertical weighting factor w_σ for these surface-layer observations is defined so that the vertical influence of the surface-layer observations decreases linearly through the lowest three model layers (about 250 m above ground level, AGL). Geostrophic adjustment theory suggests that wind data are retained better by the model if assimilated through several vertical layers (Barwell and Lorenc 1985; Stauffer et al. 1991).

The temporal weighting function w_t shown in the bottom of Fig. 3 and defined in Stauffer and Seaman (1990) is nonzero during a preset time window centered about the observation time t_0. It determines the time period over which the ith observation can influence the model simulation by means of (2). For this study, a half period of τ = 40 min is used for the special observations. In general, this time window can be defined as a function of the pressure level of the observation similar to the effect of the horizontal radius of influence R in (3).

Therefore, the final correction to the model solution via obs nudging reflects a weighted average of all observations during the present time window about the current time step and within some three-dimensional neighborhood of each grid point.

3. Experimental design

A set of six experiments is initialized at 0000 UTC 18 January 1990 and run for 48 h to investigate the

proposed multiscale FDDA strategy (Table 1). The first experiment is a control (CNTL) simulation without FDDA. Experiment AFDA examines the effect of assimilating only conventional, mesoalpha- and synoptic-scale data (hereafter referred to as "mesoalpha-scale data") on the CGM using the analysis-nudging approach; no FDDA is used on the FGM. These gridded analyses include 12-h rawinsonde data and 3-h surface data. The 3-h surface wind and moisture fields are assimilated throughout the model PBL as described by Stauffer et al. (1991).

Experiment BFDA assimilates only the special asynoptic mesobeta-scale data on the FGM using the obs-nudging approach, and no FDDA is used on the CGM. These special data include five supplemental rawinsondes (6 h), three profilers (hourly), four Doppler sodars (hourly), and 13 surface sites (hourly), and are mostly concentrated along a 350-km section of the Colorado River from southern Utah to its entrance into Lake Mead (Fig. 4). The standard rawinsonde data located within the FGM (Winslow, Arizona, Ely, Nevada, and Grand Junction, Colorado) were also included in this special obs-nudging dataset, although their coarse 12-h temporal resolution seriously limited their role in the data assimilation, compared to the special field-study data.

Multiscale FDDA experiment CFDA combines both the mesoalpha-scale analysis nudging on the 30-km CGM and the mesobeta-scale obs nudging on the 10-km FGM. The effect of assimilating the conventional mesoalpha-scale data on the CGM enters the FGM only through the nest interface.

Experiments DFDA and EFDA are similar to Experiment CFDA except DFDA uses mesoalpha-scale analysis nudging on the FGM instead of the mesobeta-scale obs nudging, and EFDA uses both mesoalpha-scale analysis nudging and mesobeta-scale obs nudging on the FGM. Thus in these two FDDA applications the mesoalpha-scale information is applied directly to the FGM domain, as well as to the CGM domain. The special mesobeta-scale dataset provides for an independent verification of the effect of assimilating this coarse-resolution (mesoalpha scale) information on the mesobeta-scale FGM in DFDA but not in EFDA where these data are directly assimilated on the FGM. Similarly, these special data allow an independent mesobeta-scale verification to be performed for CNTL and AFDA, but model evaluation is necessarily more difficult for BFDA and CFDA.

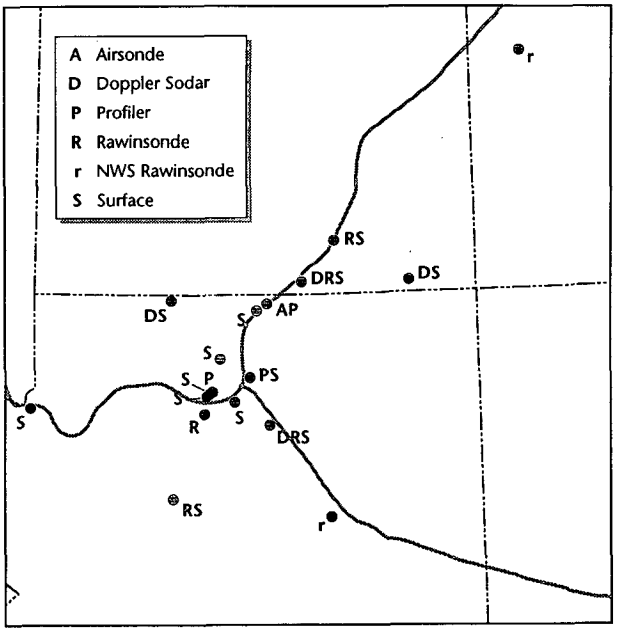

FIG. 4. Distribution and type of special data used for obs nudging on the mesobeta-scale fine-grid mesh.

TABLE 1. Experiment design.

Experiment	CGM	FGM
CNTL	—	—
AFDA	AND	—
BFDA	—	OND
CFDA	AND	OND
DFDA	AND	AND
EFDA	AND	AND, OND

Analysis-nudging design (AND)			Obs-nudging design (OND)	
3D 12-h rawinsondes	2D 3-h Surface data	Factor G (10^{-4} s^{-1})	Special asynoptic data[a]	Factor G (10^{-4} s^{-1})
u^b,v^b,T^b	u^c,v^c,q^c	2.5	u,v,T^b,q^b	4.0
q^1		0.1		

[a] Five rawinsondes (6 h), four Doppler sodars (1 h), three radar profilers (1 h), and 13 surface sites (1 h).
[b] Assimilate data above the PBL only.
[c] Assimilate data in the PBL only (Stauffer et al. 1991).

It would be desirable to withhold some of the special data from the data assimilation to allow independent verification for *all* experiments but there were not enough data with sufficient areal coverage to do this effectively (refer to Fig. 4). This is especially true for temperature and moisture data above the surface. Therefore, in addition to a statistical evaluation of the FGM solutions compared to the special data, several types of subjective evaluations, including surface-layer streamline analyses, time–height series, and back trajectories, are also performed. Both mesoalpha-scale and mesobeta-scale structures are studied in the model solutions and compared to available data on both scales. Thus the success of the various experimental designs in Table 1 is determined based on several different types of objective and subjective evaluations.

4. Case description

The case study period is from 0000 UTC 18 January 1990 (00/18) to 0000 UTC 20 January 1990 (00/20).

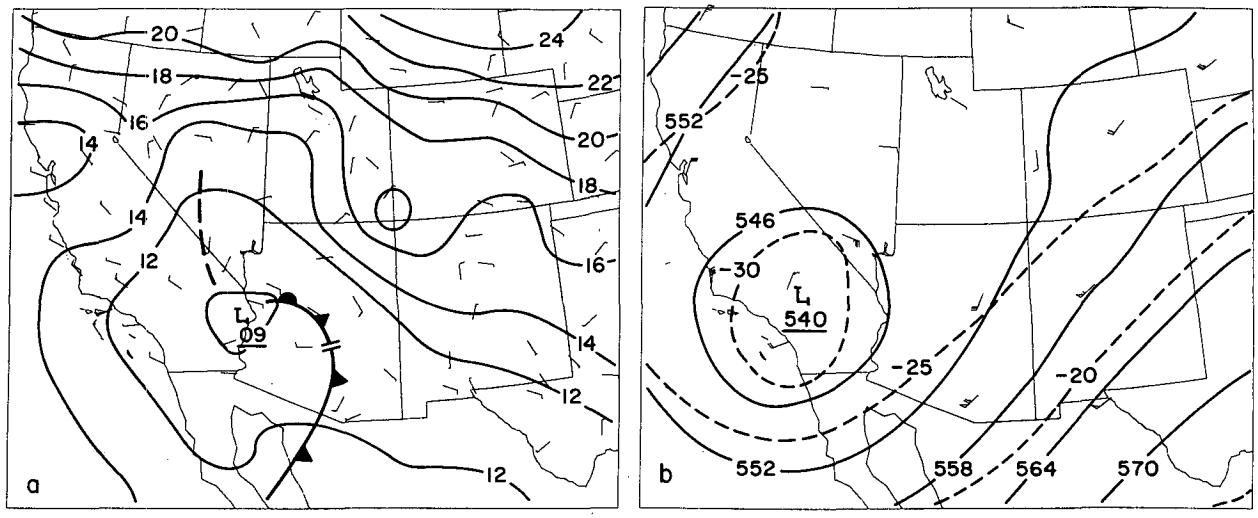

FIG. 5. Analysis of (a) sea level pressure (mb) and surface winds (one full barb is 5 m s^{-1}) and (b) 500-mb height (dam), temperature (°C), and winds at 0000 UTC 18 January 1990. The contour interval for sea level pressure is 2 mb. The contour intervals for 500-mb height and temperature are 6 dam and 5°C, respectively.

At 00/18, a weak 1009-mb winter storm was located in southern California near the Arizona border. Figure 5 shows that the surface system lay beneath a closed 500-mb cyclone. Some light rain and snow were associated with the frontal band running through south-central Arizona and also to the north of the low center in southern Nevada. Surface winds in the fine-grid domain at 00/18 (not shown) were generally light (2–6 m s^{-1}) and cyclonic to the south of the Grand Canyon; winds at Winslow, Arizona, were southerly, turning to east-northeasterly over the Grand Canyon, and then northeasterly at Page, Arizona, and throughout southern Utah.

By 12/19, the upper-level trough axis had moved eastward through the Grand Canyon region and the 500-mb low center was over southeastern Arizona (not shown). The surface low had weakened to 1011 mb over the high plateau region and was centered in the Monument Valley of northeastern Arizona, about 100 km southwest of Four Corners. Figure 6 shows that the low-level winds over the Grand Canyon region and Kaibab Plateau (refer to Fig. 2) at this time had become generally northwesterly ranging from 1 to 5 m s^{-1}, while the winds to the south of the canyon were also weak, but out of the west or southwest. Winslow, Arizona, to the east of the Mogollon Plateau, reported southwesterly surface winds at 5 m s^{-1}.

The gridded analyses, based on only conventional surface and rawinsonde data (not shown), used for analysis nudging (Experiments AFDA, CFDA, DFDA, and EFDA) are reasonably representative of the *mesoalpha-scale* flow but cannot adequately reflect the mesobeta-scale effects of the terrain. For example, the surface winds at Page, Arizona, at 12/19 (Fig. 6) were northwesterly and exceeded 5 m s^{-1} in a region where the larger-scale flow was generally weak with a possible easterly component. The special wind profiler data at Page indicate that the winds within the lowest kilometer were increasing in speed through the night (00/19 to 12/19) while turning from a northeasterly direction to a northwesterly direction by morning (see Fig. 8). However, the 700-mb winds, representing the larger-scale flow, were generally northeasterly throughout this period because the upper-level trough axis was still to the west of Page at 12/19 (see Fig. 9). After sunrise on 19 January, the low-level winds in this region be-

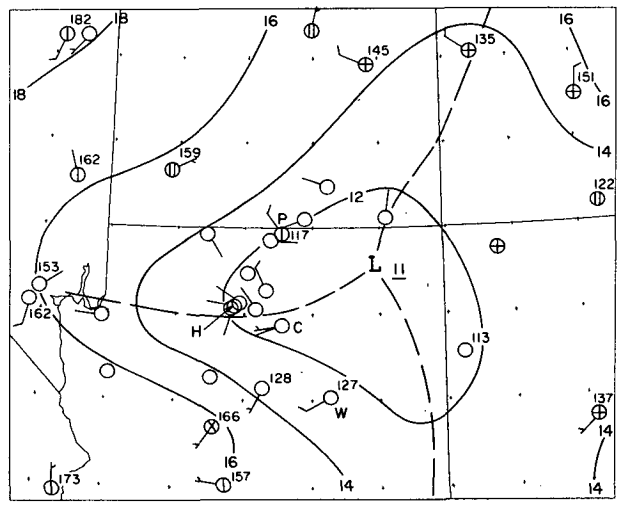

FIG. 6. Analysis of sea level pressure (mb) and surface wind (one full barb is 5 m s^{-1}) at 1200 UTC 19 January 1990. Plotted winds include both standard data and special data (see Fig. 4): *P* denotes Page, Arizona; *H* is Hopi Point, Arizona; *C* is Cameron, Arizona; and *W* is Winslow, Arizona.

came weak and west-southwesterly. Therefore, the enhanced low-level northwesterly flow at Page at 12/19 appears to be a mesobeta-scale feature probably associated with drainage winds from the Wasatch Mountains to the northwest.

By 00/20, the 500-mb cutoff low and trough axis had moved to the Oklahoma Panhandle (not shown). The weak winter storm circulation had completely dissipated over the Southwest and the low-level west-southwesterly flow had gradually increased in speed while spreading across Arizona and New Mexico.

5. Results of numerical experiments

Verification of experimental results will focus on the simulated low-level wind fields over the FGM domain and will include surface-layer streamlines, time–height series, model trajectories, and a statistical analysis of model performance at the special observation sites.

a. Surface-layer streamlines

Figure 7 shows the 36-h (12/19) simulated surface-layer streamlines from experiments CNTL, AFDA, BFDA, CFDA, DFDA, and EFDA (see Table 1). The low-level flow from CNTL (no FDDA) is shown in Fig. 7a with the local observations superimposed. Comparison with the surface analysis at this time (Fig. 6) reveals some significant problems in the CNTL simulation as the low weakened over the plateau region. The cyclonic wind vortex to the north of Winslow, Arizona, is displaced about 100 km south-southwest of the analyzed surface low. This places it closer to the upper-level low than was observed; the analyzed position of the 500-mb cutoff at this time was in southeastern Arizona with the trough axis oriented to the northwest between the Grand Canyon and Page (not shown). This phase error in the surface system has serious consequences for the low-level mesoscale flow. The winds across northeastern Arizona are simulated to be easterly instead of west-southwesterly. More importantly for this study, the winds in the Grand Canyon region and the Kaibab Plateau (refer to Fig. 2) are northeasterly at 3–10 m s^{-1}, whereas the data (Fig. 6) indicate northwesterlies at about 1–5 m s^{-1}. Despite these problems, the CNTL experiment has correctly simulated many of the general characteristics of the synoptic pattern, including the east-northeastward motion of the low center and the spread of west-southwesterly winds across the Mogollon Plateau (west of Winslow) behind the storm.

Experiment AFDA (Fig. 7b, analysis nudging on CGM only) produced some substantial improvements in the surface-layer wind solutions, compared to CNTL. In particular, the wind circulation center was moved north-northeastward very close to the surface pressure center in Monument Valley (Fig. 6). This change led to southwesterly winds across most of northeastern Arizona. Closer to Grand Canyon, however, the improvements were not as clear. Northeasterly winds persisted along the Colorado River just north of Page. Over the Grand Canyon and the Kaibito Plateau, winds were correctly turned to northwesterly but speeds were too high (about 4–7 m s^{-1}). Thus, mesoalpha-scale analysis nudging, applied only through the boundaries of the FGM, was mostly successful for improving the larger-scale flow in the region but could not reproduce many details of the mesobeta-scale flow near the Grand Canyon.

Experiment BFDA (Fig. 7c, obs-nudging on the FGM only) was most effective near the Grand Canyon where the special data were concentrated but was unable to correct most of the principal mesoalpha-scale problems noted in CNTL. For example, BFDA failed to significantly improve the position of the storm circulation. Near the canyon, the most notable improvement was a reduction of wind speed to about 2–4 m s^{-1} and a shift of the mean direction toward the northwest. Some evidence was found that the winds were affected positively in regions some distance downstream from the observations (e.g., low-level westerly wind components extend eastward onto the Kaibito Plateau), but in general the failure to also correct errors in the mesoalpha-scale flow led to only partial success of the mesobeta-scale FDDA near the canyon.

Figure 7d shows the 36-h simulated surface-layer streamlines for multiscale FDDA experiment CFDA (mesoalpha-scale analysis nudging on the CGM plus mesobeta-scale obs nudging on the FGM). First, the surface-low wind circulation center has been correctly shifted to the Monument Valley southwest of Four Corners, and the winds in northeastern Arizona now have a westerly component rather than easterly. These larger-scale improvements outside the special observations network resulted from the mesoalpha-scale analysis nudging on the CGM, which improved the lateral boundary conditions supplied to the FGM. This can be seen by comparing the results from CFDA with AFDA (Fig. 7b). Of equal importance, the winds near the Grand Canyon have also been corrected to mostly northwesterly and reduced to about 2–4 m s^{-1}. Comparison with the observations indicates fairly good agreement at most sites.

However, at Cameron, Arizona (about 100 km northwest of Winslow along the river, see Fig. 2), the northwesterly flow in CFDA was extended too far to the southeast of the canyon region. Although it is weaker in magnitude in CFDA than CNTL (compare the shading, which indicates wind speeds exceeding 5 m s^{-1}, in Figs. 7a and 7d), horizontal advection and channeling by the Little Colorado River valley tended to favor this direction. Also, the three northwesterly wind observations to the northwest of Cameron are within R_s = 100 km and partially offset the effect of the west-southwesterly Cameron observation in the local obs-nudging compu-

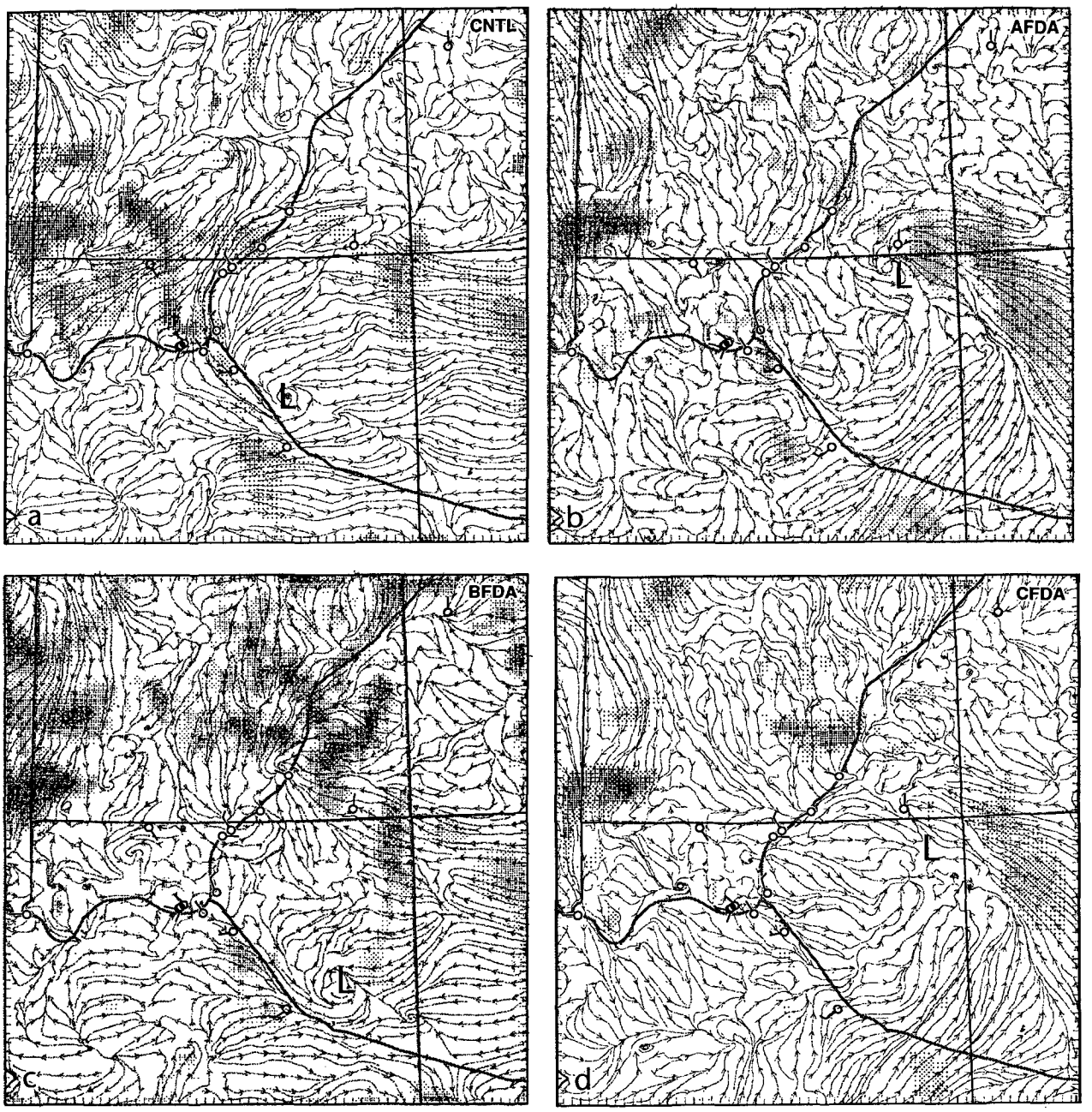

FIG. 7. Numerically simulated surface-layer (35 m AGL) streamlines at 36 h (1200 UTC 19 January 1990). The geographic area is identical to the one displayed in Fig. 2 and corresponds to the fine-grid mesh computational domain. The *L* denotes the circulation center of the storm near the surface. The special field study observations near the surface are located mainly along the Colorado and Little Colorado Rivers (heavy solid lines), and one full-length wind barb is 5 m s^{-1}. The shading indicates regions with *model-simulated* wind speeds in excess of 5 m s^{-1}: (a) CNTL, (b) AFDA, (c) BFDA, (d) CFDA, (e) DFDA, and (f) EFDA.

tations. Only 20 km farther south, the CFDA winds become more westerly, reflecting the stronger influence of the Cameron observation in the FDDA. This demonstrates the potential problems associated with nonuniform data density and "representativeness" uncertainties. (One possible way to minimize these problems is to use a "super observation" approach: in this case the canyon region could be represented by one composite observation that carries the same weight as the single Cameron observation.) Nevertheless, these problems were mainly limited to the Cameron area, and the overall impact of the special data was clearly more effective in this experiment than in BFDA.

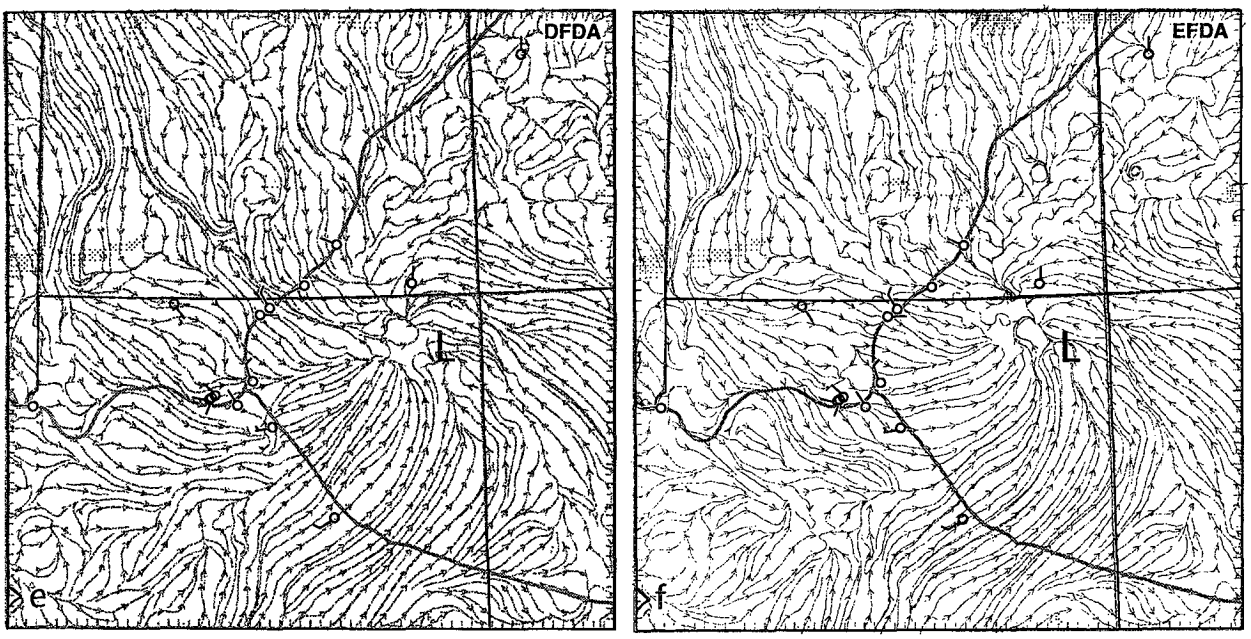

FIG. 7. (*Continued*)

The west-southwesterly flow pattern indicated by the Cameron observation persisted for 6 h and appears to be more representative of the *mesoalpha-scale* circulation. This may be explained by Cameron's location, which is farther east of the Kaibab and Mogollon Plateaus than any other observation in the canyon region (refer to Figs. 2 and 4), and is therefore more representative of the Painted Desert region and thus the larger-scale wind pattern. The Cameron area was best simulated on the FGM in those experiments that assimilated mesoalpha-scale information (AFDA, Fig. 7b; DFDA, Fig. 7e; EFDA, Fig. 7f). The importance of mesoalpha-scale forcing at Cameron is further suggested by the BFDA results (Fig. 7c), which, like the CNTL, simulated a northwesterly flow throughout this region, despite the mesobeta-scale obs nudging on the FGM. In CFDA, the FGM obs nudging is more effective due to the complementary influence of the mesoalpha-scale analysis nudging on the CGM entering the FGM through the lateral boundary conditions.

There is also evidence in these experiments that mesobeta-scale terrain influences remain important for modifying the mesoalpha-scale flow, especially in regions away from the special observations network. That is, the FDDA scheme is not adversely affecting the model's natural ability to produce realistic mesobeta-scale features in data-sparse regions. For example, in CFDA the northwesterly flow in Utah is deflected around the southern end of the Wasatch Mountains and there is locally confluent flow along nearly the entire length of the Colorado River (Fig. 7d). Also, drainage flows are clearly evident in several valleys in the northeastern part of the FGM. In section 5b, simulation of drainage winds from the Wasatch Mountains will be investigated using time–height section analyses at the Page profiler site and model trajectories.

Since none of these mesobeta-scale details were evident in the mesoalpha-scale analyses, nor were there sufficient data to force them into the solution, except in the central data-rich area close to the canyon, these results illustrate the advantage of combining a dynamic model solution and data through FDDA. However, it is also possible that a mesoscale simulation with FDDA is worse than one without FDDA when the data used for assimilation represent scales much larger than those resolved by the model grid.

This is a very important issue, particularly when the finer-scale data cover only a portion of the finescale domain or are simply not available. The implications may be quite different for gridpoint models like the one used here, as compared to spectral models in which the scales directly affected by data assimilation can be explicitly controlled (Krishnamurti et al. 1988). This is much more difficult to accomplish in gridpoint space. Scale separation via Fourier decomposition is possible in limited-area gridpoint models (Errico 1985) but may not be practical for FDDA applications. The scale separation problem is addressed here via the grid-nesting scheme and the different FDDA strategies used on each mesh.

To investigate the effect of assimilating coarse-resolution data on a finescale grid, we will compare experiments AFDA (no FGM FDDA, Fig. 7b), CFDA (mesobeta-scale FGM FDDA, Fig. 7d), DFDA (mesoalpha-scale FGM FDDA, Fig. 7e), and EFDA (both mesoalpha-scale and mesobeta-scale FGM FDDA, Fig.

7f). There were very few grid points with winds exceeding 5 m s^{-1} in the FGM mesoalpha-scale wind analysis at this time (not shown). Relaxation of the model FGM winds in DFDA and EFDA to this gridded dataset has reduced the wind speeds over the entire FGM as compared to the other experiments, as expected. This is not to say that there are no mesobeta-scale features present in the DFDA and EFDA simulations but they are much weaker in amplitude due to the assimilation of a dataset that lacks mesobeta-scale structure. Although combining the mesoalpha-scale analysis nudging with mesobeta-scale obs nudging on the FGM (experiments EFDA) does produce more finescale structure than using only mesoalpha-scale analyses (experiment DFDA), it also partially offsets the ability of the obs nudging to introduce the finescale structure on the FGM (compare experiments EFDA and CFDA). Despite the obvious improvements in the larger-scale character of the flows at 36 h (e.g., the low center), the ability of a mesoscale gridpoint model to generate finer-scale detail (drainage winds, channeling, etc.) is therefore somewhat limited when assimilating a dataset of much coarser resolution. Thus, analysis-nudging FDDA can have a *negative* impact on a simulation if coarse-resolution data are applied directly to a much finer-scale grid, especially when there is strong finescale forcing, such as that associated with complex terrain. This will be investigated further using time–height section analyses.

b. Time–height series and trajectory analysis

Time–height series and model trajectories are used together in this section to investigate the time-integrated effects of the various FDDA strategies. Figure 8 shows the observed and simulated low-level wind fields for the second day, 19 January, at the Page, Arizona, profiler site. As mentioned in section 4, the profiler winds at Page show the development of an enhanced low-level northwesterly flow through the nighttime hours on the second day (06/19–12/19). The observed time–height series (Fig. 8a) shows three different wind regimes: 1) from 24 to about 30 h, large-scale northeasterly flow associated with the mesoalpha-scale pattern; 2) from 31 to about 38 h, a northwesterly mesobeta-scale nocturnal drainage flow from the Wasatch Mountains to the northwest of Page; and 3) from 39 to 48 h, a return to large-scale flow conditions with weak westerlies gradually increasing in speed with time as the low passed through northeastern Arizona.

Mesoalpha-scale phase errors in the movement of the low and channeling of the erroneous wind by the terrain produced strong, persistent east-northeasterly winds at Page in CNTL (Fig. 8b) from 24 through 36 h. The northwesterly drainage winds never developed, and the shift to westerly flow did not occur until 44 h. Mesoalpha-scale analysis nudging on the CGM in AFDA (Fig. 8c) significantly reduced the magnitude

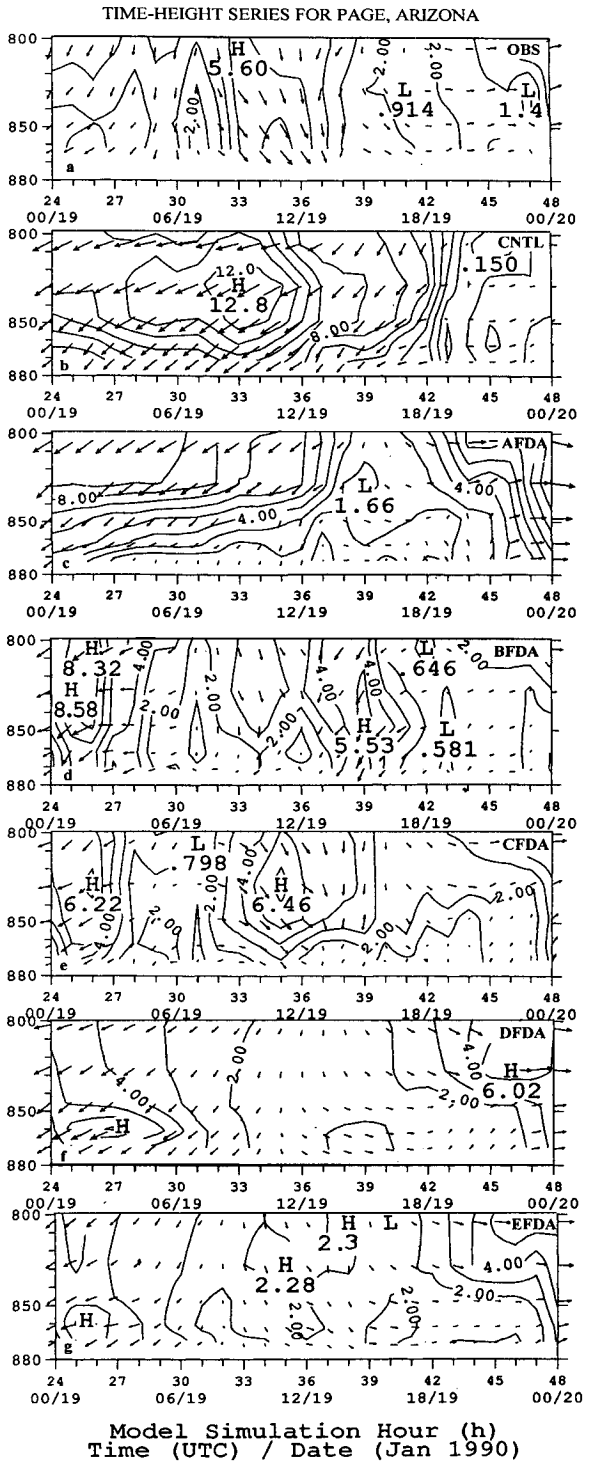

FIG. 8. Time–height series of wind within the lowest 1 km at the Page, Arizona, profiler site from 24 h (0000 UTC 19 January 1990) to 48 h (0000 UTC 20 January 1990). The contour interval of the isotachs is 1 m s^{-1}: (a) observed, (b) CNTL, (c) AFDA, (d) BFDA, (e) CFDA, (f) DFDA, and (g) EFDA.

of the northeasterly flow on the FGM at Page from 24 to 36 h but was still unable to develop the northwesterly drainage winds. By 38 h the AFDA winds shifted to westerly, as observed, and increased in speed through 48 h.

The special mesobeta-scale observations are directly assimilated via obs nudging on the FGM in experiment BFDA (Fig. 8d). A northwesterly low-level flow is simulated by 32 h, but it is too weak and fails to reach the surface. Also the strong low-level northeasterly winds produced by BFDA at 39 h were not observed. Recall that the assimilation of the localized mesobeta-scale observations was unable to overcome the mesoalpha-scale errors of the CNTL, related to the position of the low, and so was only partially successful. By complementing the FGM obs nudging with mesoalpha-scale analysis nudging on the CGM, experiment CFDA (Fig. 8e) extended the nocturnal northwesterly winds to the surface from 33 to 37 h and produced a drainage flow closer in magnitude to that observed. Therefore, the obs nudging at the mesobeta scale was made more effective by simply improving the FGM boundary values through FDDA on the CGM, which reduced the mesoalpha-scale errors.

Experiment DFDA (Fig. 8f) directly assimilated the coarse-resolution mesoalpha-scale analyses on both the CGM and FGM. Although the northeasterly winds are further reduced in magnitude at Page at 31 h compared to AFDA (Fig. 8c), the northwesterly drainage flow was still absent. Assimilation of both mesoalpha-scale and mesobeta-scale data on the FGM (experiment EFDA, Fig. 8g) did produce northwesterly drainage winds at the surface by 35 h but they are much weaker than those in CFDA, which assimilated only mesobeta-scale data on the FGM. In EFDA the coarse-resolution analysis nudging on the FGM acted as a filter or smoother on this mesobeta-scale feature.

Figure 9 shows time series of 700-mb wind, representing the larger-scale wind patterns, at Page, Arizona, during the same period as in Fig. 8. The Page profiler (PRFOBS) showed that a shift from northeasterly to northwesterly flow occurred after 42 h (18/19), and this was associated with the passage of the trough axis extending northwestward behind the 500-mb cutoff low. However, the 12-h rawinsonde analyses (RAWANL) showed weak northwesterly flow at 700 mb over Page at 36 h (12/19) and indicated that the trough passage had already occurred by this time. This erroneous result is due to the spatial smearing caused by the poor spatial resolution of the standard rawinsonde network in the vicinity of Page. Page is located almost midway between the upper-air stations at Ely, Nevada; Grand Junction, Colorado; and Winslow, Arizona. This shows that rawinsonde data have inherent limitations even on the synoptic scale.

Experiment CNTL simulated the latest time of trough passage (47 h), while DFDA, which assimilated these rawinsonde analyses over the FGM, had the earliest (37 h). Experiment EFDA, which assimilated both rawinsonde analyses and the special mesobeta-scale dataset (including the Page profiler) over the FGM, still simulated the 700-mb wind shift to occur too early (39 h). Thus, similar to what happened with the drainage winds at the surface, the coarse-resolution analysis nudging is offsetting the effect of the mesobeta-scale obs nudging (e.g., see experiments BFDA and CFDA). Thus, assimilation of analyses with poor spatial and temporal resolution can contribute to failures in simulating the timing of even large-scale midtropospheric features.

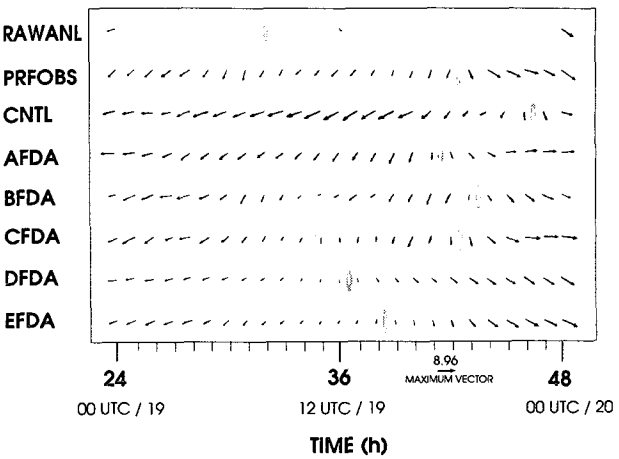

FIG. 9. Time series of 700-mb wind, depicting the evolution of the large-scale wind pattern at the Page, Arizona, profiler site from 24 h (0000 UTC 19 January 1990) to 48 h (0000 UTC 20 January 1990). Gray ellipses mark the time of the wind shift associated with the midtropospheric trough passage. RAWANL denotes rawinsonde analyses at the Page location, and PRFOBS denotes the Page radar profiler. See Table 1 for description of each model experiment.

On the other hand, experiments AFDA, BFDA, and CFDA all simulated the timing of the trough passage within 1 h of when it was observed at the Page profiler site. Experiment AFDA, which had no FDDA on the FGM (and thus no bad analysis-nudging contribution), improved the timing of the wind shift compared to CNTL by means of the lateral boundary conditions and analysis nudging on the CGM. Although both BFDA and CFDA directly assimilated the Page profiler data, multiscale FDDA experiment CFDA verified best of all experiments by simulating the wind shift to occur within the same hour as the Page profiler.

Thus this time series analysis at Page demonstrates the importance of adequate *spatial and temporal* resolution in the data used for FDDA, not only for simulating mesobeta-scale features such as drainage winds but also for mesoalpha-scale features such as midtropospheric troughs. The multiscale FDDA experiment CFDA produced the most realistic simulation of these two features of all the experiments by assimilating mesobeta-scale information on the FGM and mesoalpha-scale information on the CGM.

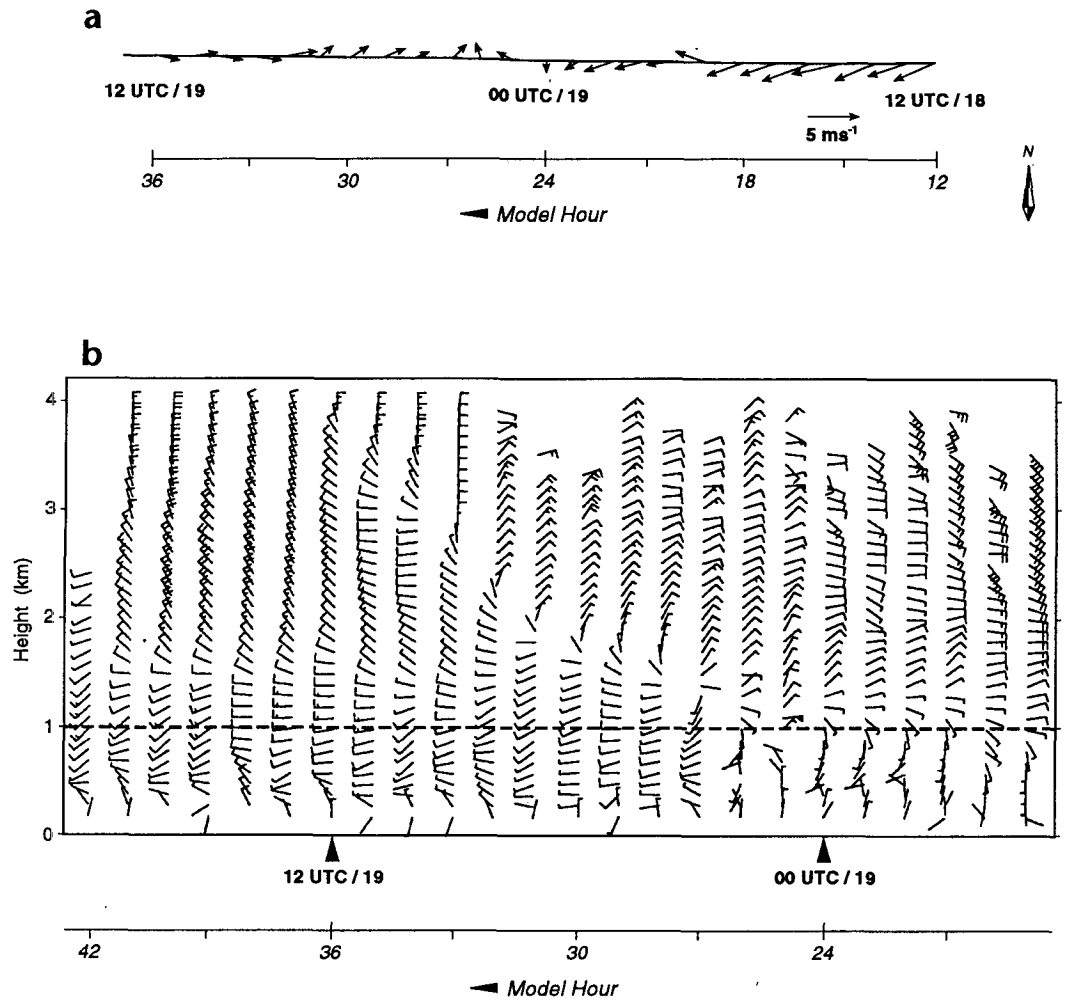

FIG. 10. Time series of observed winds at (a) surface site, Hopi Point, Arizona, and (b) nearby profiler site, Phantom Ranch, Arizona, located within the Grand Canyon. In (b), one full barb is 5 m s^{-1} and the heavy dashed line reflects the "canyon rim" and the model terrain height.

Model-based trajectories are useful for comparing the time-integrated Lagrangian effects (i.e., following the parcel) of the various FDDA strategies. The sensitivity of model trajectories (transport) to FDDA is especially important for air pollution applications. The 36-h time is chosen here for calculation of "back trajectories" (backward in time) because differences among the experiments were greatest at this time due to the rapidly changing mesoalpha- and mesobeta-scale conditions (refer to Figs. 7–9). Back trajectories are computed from the following three locations (refer to Fig. 2): Page, Arizona (parcel A); Hopi Point, Arizona (parcel B); and at 36°N, 110°W over the Black Mesa in northeastern Arizona (parcel C). Parcel A is used to further investigate the effects of FDDA on the simulation of the mesobeta-scale drainage flow observed at Page. Parcel B traces the origin of the air over the relatively data-rich Grand Canyon region, while parcel C is used to compare the effects of FDDA on the flow in the *data-void* region to the east of the special observation network.

Although there were no tetroon data available for this study, chemical tracer and emittants released from the Navajo Generating Station (NGS), located near Page, were detected at Hopi Point in the Grand Canyon region during this period (Kessler 1992, personal communication; Richards 1992, personal communication). Model back trajectories can also be qualitatively compared against the special data set and the mesoalpha-scale analyses to assess their general skill. The Page profiler winds at *A* were shown in the time–height series in Fig. 8a, while special wind data over the Grand Canyon are shown in Fig. 10. Figure 10a shows a time series of surface winds at Hopi Point (*B*), and Fig. 10b shows the time–height series of winds for a nearby profiler site at Phantom Ranch, which is actually located within the canyon. The model terrain in this region is about 1 km higher than the elevation at Phantom

Ranch (750 m) within the canyon. Thus the winds within the lowest kilometer of Fig. 10b must be ignored here because they are below the rim of the canyon, which of course is not resolved by the 10-km mesh. No data are available at Black Mesa (*C*).

Figure 11 shows the back trajectories (i.e., backward-in-time paths) taken during the past 36 h by air parcels arriving in the surface layer (35 m AGL) at these three locations for each of the five experiments. The arrowheads indicate the direction in which an air parcel is being advected by the model winds and also mark its displacement every 6 h. The vertical displacements along the trajectories are not shown, because they are typically less than 500 m. That is, the parcels generally follow the terrain and stay within the PBL. Figure 11, therefore, indicates the model-predicted source regions for these three parcels. (Because the trajectories from EFDA were generally very similar to those from DFDA, they are not shown in Fig. 11.)

For example, the surface-layer air arriving at Page (point *A*) at 36 h in CNTL (Fig. 11a) was simulated to originate in northeastern New Mexico 36 h earlier (00/18). At 30 h (6 h earlier, 06/19), it was located about 120 km to the northeast of Page. However, from 30 to 36 h, the observed low-level flow at Page was from the northwest (drainage winds, Fig. 8a). Because of the clearly erroneous flow near Page during this final 6 h, the simulation of the source region for parcel A in CNTL is suspect. Experiment CFDA (Fig. 11b) is the only experiment in which the parcel A position at 30 h is to the northwest of Page, as suggested by the data; the other experiments all show 30-h positions to the northeast of Page. Experiment BFDA (which like CFDA also assimilated mesobeta-scale data) failed to compute the trajectory into Page (point *A* in Fig. 11) from the northwest because the drainage winds were too weak and failed to reach the surface without the complementary mesoalpha-scale analysis nudging (refer to Fig. 8). Note that the source regions at 0 h (00/18) among the various experiments are very different. This, of course, has serious implications for air quality studies.

The CNTL parcel (Fig. 11a) arriving at Hopi Point (*B*) in the Grand Canyon region at 36 h was simulated to be more than 150 km northeast of the canyon only 6 h earlier. Although its path would be consistent with data showing tracer constituents released from NGS reaching Hopi Point, the surface wind data at Hopi Point (Fig. 10a) suggest that the parcel should have arrived at *B* from the west. Furthermore, due to the light winds observed there (1–2 m s^{-1}), which were also changing direction from 24 to 36 h (00/19–12/19), the corresponding 24–36-h parcel displacement should be relatively small (20–50 km). The displacement from 12 to 24 h (12/18–00/19), on the other hand, would be much larger due to stronger and persistent northeasterly flow through this period in the larger region. The CFDA back trajectory (Fig. 11b) from Hopi Point (*B*) is consistent with these data, including a displacement of only about 30–40 km during the final 12 h, and like CNTL, it also followed a path that passed by Page and NGS. Similar to CNTL, however, both AFDA (Fig. 11c) and BFDA (Fig. 11d) show the parcel arriving at *B* from the north or northeast. Although experiments DFDA (Fig. 11e) and EFDA (not shown) also have the parcel arriving at *B* from the west, there is no sign of the wind shifting through south along its back trajectory, as was seen in both the data (Fig. 10a) and the CFDA back trajectory (Fig. 11b). Therefore, the multiscale FDDA strategy (experiment CFDA) was the only experiment to produce model back trajectories that were consistent with the data at both Page (*A*) and Hopi Point (*B*).

The air arriving at Black Mesa (*C*) at 36 h is south of the analyzed surface low (refer to Fig. 6) where a westerly wind component would be expected in the final hours before 12/19. The CNTL (Fig. 11a) shows the parcel arriving at *C* from the east due to the phase error in the surface low at this time, as discussed earlier. The CFDA back trajectory (Fig. 11b) from *C* correctly shows the parcel arriving from the southwesterly direction at 36 h after having followed a generally cyclonic path over the previous 36 h as it was advected through Monument Valley along the eastern side of Black Mesa (refer to Fig. 2). The mesoalpha-scale effects of the analysis nudging on the CGM were introduced onto the FGM through the nest interface. The analysis nudging greatly affected the parcel paths to *C* in both CFDA (Fig. 11b) and AFDA (Fig. 11c), compared to CNTL (Fig. 11a) and BFDA (Fig. 11d), although mesobeta-scale channeling effects were also important. The AFDA back trajectory from *C* is similar to CFDA except that the parcel arrived from the western side of Black Mesa after passing through Monument Valley, and its 36-h displacement is much shorter than in CFDA. This difference in the trajectories for *C* represents the effect of obs nudging over the Grand Canyon in a downstream data-void region of the FGM. Of course, it cannot be determined if the CFDA trajectory from *C* is more accurate than that of AFDA. Nevertheless, the effect of assimilating the special data in the FGM domain on parcel paths through this data-void region was greater in CFDA (compare with AFDA) than in BFDA (compare with CNTL). Thus, in this case the multiscale FDDA strategy renders the mesobeta-scale obs nudging on the FGM to have a greater impact in both data-void and data-rich regions. Finally, experiment DFDA (Fig. 11e) shows the parcel arriving at *C* at 36 h from the southwest similar to that in CFDA (Fig. 11b), but its source region 36 h earlier is completely different from any of the other experiments (southwest New Mexico). This shows quite dramatically how sensitive model trajectory calculations can be to variations in the FDDA strategy.

Figure 12 shows back trajectories of air parcels arriving at these same three locations at 36 h from CNTL

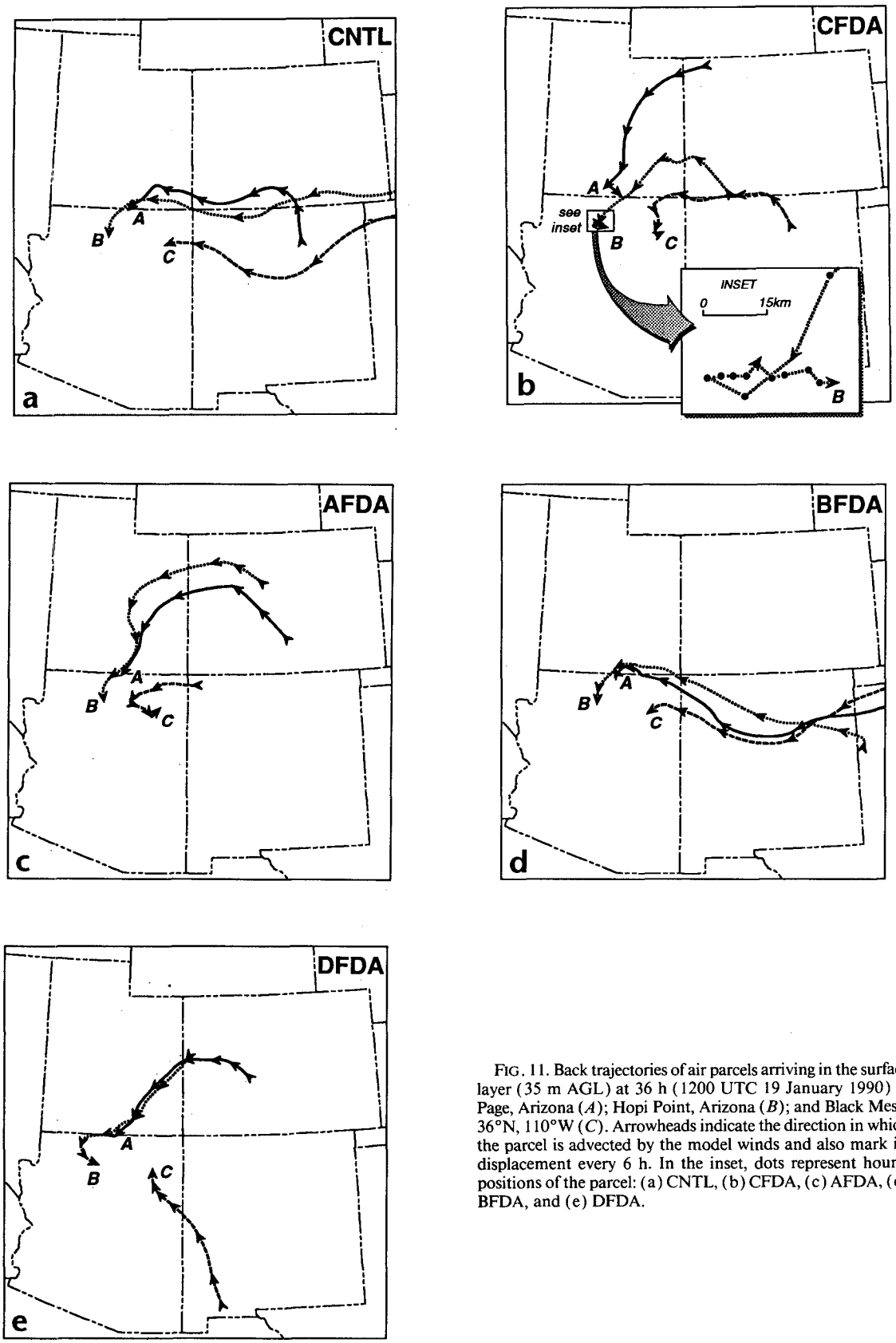

FIG. 11. Back trajectories of air parcels arriving in the surface layer (35 m AGL) at 36 h (1200 UTC 19 January 1990) at Page, Arizona (*A*); Hopi Point, Arizona (*B*); and Black Mesa, 36°N, 110°W (*C*). Arrowheads indicate the direction in which the parcel is advected by the model winds and also mark its displacement every 6 h. In the inset, dots represent hourly positions of the parcel: (a) CNTL, (b) CFDA, (c) AFDA, (d) BFDA, and (e) DFDA.

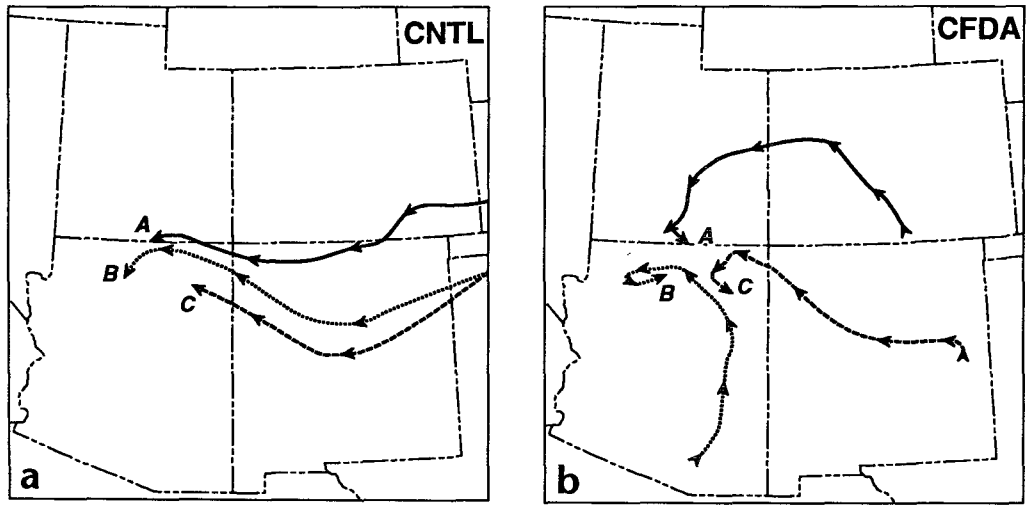

FIG. 12. As in Fig. 11 but for air parcels arriving at these three locations at about 500 m AGL: (a) CNTL, and (b) CFDA.

(Fig. 12a) and CFDA (Fig. 12b), except at about 500 m AGL. The CFDA back trajectory from *A* is again consistent with the observed northwesterly drainage flow in the several hours before 12/19 (Fig. 8a), while that from CNTL is not. Also, the effects on parcel C due to the phase error of the surface low (CNTL) and the multiscale FDDA (CFDA) are similar to those found at 35 m AGL (Figs. 11a and 11b).

The profiler data at Phantom Ranch (*B*) in Fig. 10b shows the winds were about westerly up to 1.5 km above the bottom of the canyon (i.e., 0.5 km AGL in the model) for at least 8 h prior to the final time of the trajectory calculations at 12/19. At 24 h (00/19), the observed winds were easterly or northeasterly at and above this height. Between 27 and 36 h, Fig. 10b shows that the westerly wind shift gradually grows upward with time as the trough axis moves to the east. However, Fig. 12a shows the parcel arriving at *B* in CNTL to have come from the northeast. Similarly, the parcel arriving at *B* at this time in BFDA (not shown) also arrived from the northeast. Thus, both experiments failed to produce the correct direction for the winds for at least several hours in the vicinity of the Grand Canyon. The parcel arrives at *B* from the west in CFDA (Fig. 12b) after encountering a reversal of the northeasterly flow between 24 and 30 h. This latter trajectory agrees well with the mesoalpha-scale trough and associated wind shift in the data (Fig. 10b) and further demonstrates the importance of a *multiscale* FDDA strategy.

c. *Statistical analysis*

A statistical summary of the model winds in the lowest 500 m AGL (four lowest model layers) at the special mesobeta-scale observation sites is presented in Fig. 13. The root-mean-square vector wind difference (rms VWD) errors were computed for 3-h time windows throughout the 48-h period. The FGM analysis error at $t = 0$ h (00/18) is 3.3 m s^{-1} and represents how closely a mesoalpha-scale analysis is able to "fit" the mesobeta-scale data in the vicinity of the Grand Canyon. The misplacement of the wind circulation of CNTL at 36 h (see Fig. 7) appears in Fig. 13 as a large increase in the rms errors between 30 and 42 h, due to a phase lag in establishing the northwesterly flow over the Grand Canyon as the low tracks eastward. The special observations provide an independent verification set for only experiments CNTL, AFDA, and DFDA, and the statistical results from EFDA were comparable to CFDA and are not discussed.

Figure 13 clearly shows that the CGM mesoalpha-scale nudging (experiment AFDA) effectively reduced

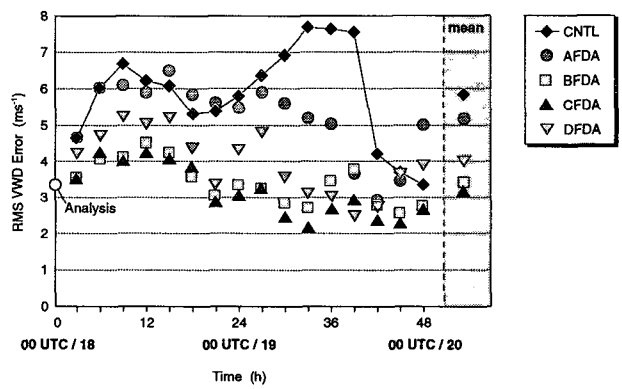

FIG. 13. Root-mean-square vector wind difference (rms VWD) errors (m s^{-1}) of model-simulated winds in the lowest 500 m AGL (lowest four model layers) at the special observation sites for the 48-h experiments.

the larger-scale phase errors during this period. Although BFDA produced a greater improvement in the statistical skill at the special observation sites throughout the simulation, inspection of the wind fields over the entire FGM (section 5a) indicated that there was still considerable error in the outlying areas. This result demonstrates the dilemma concerning the need for independent model validation that can arise with FDDA applications: The local error reduction in the vicinity of the observations is certainly very real, but without an additional nonassimilated dataset, it may be difficult to determine the overall level of skill.

Experiment CFDA, on the other hand, consistently provided the most accurate representation of the winds over the special observation network, while simultaneously controlling error growth in the outer areas of the FGM. Although experiments DFDA and EFDA (not shown) also reduced the errors at the special observation sites as compared to CNTL by improving the mesoalpha-scale character of the flow, they still failed to accurately simulate terrain-forced mesobeta-scale features (see Fig. 8). Therefore, one would expect that experiment CFDA, the model simulation that best agrees with the available data, should also provide the most accurate trajectories, at least in the region covered by the data (section 5b).

These statistics are also representative of FDDA model performance over the lowest 10 model layers (below about 2500 m AGL), where most of the special data were concentrated. Although the number of observations decreases with increasing height above the surface (see Fig. 4), the statistical results for each 500-m layer, and for the entire 2500-m layer (see Table 2), are very similar to those presented in Fig. 13.

Using the model configuration described in section 2a, the six experiments in Table 1 were repeated for a second 48-h case within the Salt River Project's special observation period (0000 UTC 26 February 1990–0000 UTC 28 February 1990). The mesoalpha-scale forcing was much weaker in this case than in the January case, but the results are similar. Table 2 also shows the 48-h case mean wind statistics for the lowest 500- and 2500-m AGL layers for the two cases. Thus, the multiscale FDDA experiment CFDA provided the most accurate simulation of the low-level wind fields in both cases.

TABLE 2. Statistical summary of model-simulated wind fields over the special observations network for case I (0000 UTC January 18 1990–0000 UTC 20 January 1990) and case II (0000 UTC 26 February 1990–0000 UTC 28 February 1990). The 48-h case-mean root-mean-square vector wind difference (rms VWD) errors (m s^{-1}) are shown for the lowest 500-m AGL layer (lowest 4 model layers) and the lowest 2500-m AGL layer (lowest 10 model layers).

	Case I		Case II	
Experiment	500 m	2500 m	500 m	2500 m
CNTL	5.8	7.2	4.3	5.1
AFDA	5.2	6.0	3.8	5.0
BFDA	3.4	3.8	2.5	2.8
CFDA	3.1	3.6	2.4	2.7
DFDA	4.0	5.1	2.8	3.8

6. Summary

Mesobeta-scale numerical modeling of real-data cases is becoming increasingly practical due to the availability of near-continuous data streams and continued growth in computing power. Continuous four-dimensional data assimilation (FDDA) schemes capable of effectively analyzing this database are needed for both model initialization and dynamic analysis.

The study of many of today's environmental problems requires high-frequency, fine-resolution meteorological datasets spanning periods of several days. Since economic constraints limit the total number of observations, however, these data are always "incomplete" and generally distributed nonuniformly in space and time. Because of such limitations and the complex relationships between the different atmospheric fields and the various scales of motion, a *dynamic* approach to data analysis and assimilation is required. Therefore, continuous FDDA by means of nudging is used here in a *mesobeta-scale* model to generate complete, dynamically consistent meteorological datasets that are suitable for input into air quality models but can also be used for other diagnostic purposes, as well as model initialization.

This paper has tested a *multiscale* nudging strategy to simulate the wind flow in two real wintertime cases over the Colorado Plateau and Grand Canyon region, with emphasis on the case of 18–20 January 1990. A special mesobeta-scale observing system had been deployed in the Grand Canyon region during that winter season, under the sponsorship of Salt River Project, to study the canyon's visibility impairment problem. The special data included Doppler sodars, profilers, rawinsondes, and surface stations. Combinations of these data and conventional data were assimilated into a nested version of the Pennsylvania State University–National Center for Atmospheric Research Mesoscale Model to investigate the importance of scale interaction and scale separation during FDDA.

One of the main objectives of this study was to determine whether FDDA is most effective on the 10-km fine-resolution domain by relying solely on conventional, mesoalpha-scale FDDA on the 30-km coarse grid to improve the time-continuous lateral boundary conditions supplied to the inner fine grid by directly assimilating the asynoptic mesobeta-scale observations on the fine grid or by a combination of these two approaches. Another objective was to study the effects of assimilating coarse-resolution mesoalpha-scale analyses directly on a fine-scale grid, either in addition to or in place of assimilation of mesobeta-scale data, to deter-

mine if the FDDA can have adverse effects on the simulation of mesobeta-scale features.

Mesoalpha-scale forcing was shown to be important for accurate simulation of the mesobeta-scale flow over the 48-h period. The use of mesoalpha-scale analysis nudging on the 30-km coarse-grid mesh with no FDDA on the 10-km fine-grid mesh (experiment AFDA) was generally effective for reducing the larger-scale errors on the fine-grid mesh but had a much smaller effect on the mesobeta-scale errors. Assimilation of only the special mesobeta-scale information on the 10-km fine grid via obs nudging with no FDDA on the 30-km coarse grid (experiment BFDA) had limited success on the mesobeta scale and very little effect on correcting the mesoalpha-scale errors outside the special observations network (e.g., the movement of the surface low).

In experiment CFDA, the use of mesoalpha-scale FDDA on the 30-km coarse grid, which contributed to the reduction of mesoalpha-scale errors on the 10-km fine grid through the lateral boundaries enabled the mesobeta-scale obs nudging to be more effective than in experiment BFDA. This multiscale FDDA strategy was successful in correcting many local aspects of the flow in areas where the special data were available. The FDDA did not, however, "overwhelm" the model's dynamics or prevent it from producing a reasonable solution in data-sparse regions of the fine-grid mesh. For example, realistic channeling and drainage flows were simulated outside the special observations network while mesoalpha-scale errors related to the motion of the winter cyclone were simultaneously reduced. The movement of the weak winter storm circulation in northeastern Arizona, to the east of the special observations network, was much improved on the fine-grid mesh by the analysis-nudging FDDA applied on the coarse-grid mesh. Comparisons of the wind fields on the 10-km fine grid, using both subjective and statistical measures, including trajectories, indicate that this multiscale approach was the most effective data-assimilation strategy.

Finally, direct assimilation of coarse-resolution, mesoalpha-scale analyses on the mesobeta-scale fine-grid mesh, either with or without mesobeta-scale FDDA (experiments EFDA and DFDA, respectively), had both some advantageous and adverse effects on the simulation for both the mesobeta and mesoalpha scales. Although both experiments reduced the statistical vector wind errors on the fine-grid mesh compared to experiment AFDA, the surface-layer streamlines and time–height section analyses showed that *mesobeta-scale* features were either absent or significantly reduced in amplitude. Combining mesobeta-scale obs nudging and mesoalpha-scale analysis nudging on the same mesh in experiment EFDA showed that even though the analysis-nudging coefficient ($G = 2.5 \times 10^{-4}$ s^{-1}) was smaller than that for obs nudging ($G = 4 \times 10^{-4}$ s^{-1}) the amplitude of the mesobeta-scale features was greatly reduced; the assimilation of the mesoalpha-scale analyses on the FGM acted like a filter or smoother on the mesobeta-scale structure. Whenever there is likely to be a strong finescale component to the numerical solution, assimilation of relatively coarse-resolution (space and/or time) gridded data can do more harm than good by limiting the model's natural ability to produce finer-scale features, which may be absent or marginally resolved in the gridded analyses used for FDDA.

In this case, the coarse spatial and temporal resolution of the rawinsonde analyses also adversely affected the DFDA and EFDA *mesoalpha-scale* solutions: the wind shift associated with the passage of the upper-level trough was forced to occur many hours too early in both experiments. To be effective, the gridded data used for analysis-nudging FDDA must adequately represent the resolvable scales on whatever model grid the assimilation scheme is applied. Further reduction of the analysis-nudging weights on the fine grid would help restore the mesobeta-scale features but would render the FDDA less effective in areas where the mesoalpha-scale forcing is important. Ideally, to use both mesoalpha-scale analysis nudging and mesobeta-scale obs nudging on the same mesh, one could define the obs-nudging (analysis-nudging) weights to be large (small) where mesobeta-scale forcing is dominant and small (large) where mesoalpha-scale effects are important. This, of course, is very difficult to do, especially in the general case where the mesobeta-scale features are moving and not associated with the topography (e.g., convective outflow boundaries). In the future, adjoint methods may be useful for determining the optimal values of these nudging coefficients (e.g., Stauffer and Bao 1993).

Therefore, for gridpoint models, the use of grid nesting to separate the mesoalpha-scale and mesobeta-scale FDDA is easier and more effective than attempting both on the same grid. In finescale simulations, observations should be assimilated directly with appropriate weighting functions rather than as gridded analyses. When designing an FDDA strategy, scale interactions of different flow regimes cannot be ignored, particularly for simulation periods of several days on the mesobeta scale. Although controlling error growth on the mesoalpha scale does not guarantee success on the mesobeta scale, this grid-nesting, multiscale FDDA approach has been shown to allow the *mesobeta-scale* FDDA to be more effective.

Acknowledgments. This work was supported by the Salt River Project through Award VN08021CAS and NSF Grant ATM-9116176, with additional support from DOE Contract DE-FG02-90ER61071 and NSF/FAA Grant ATM-9203317. Annette Lario, James Hegarty, and Scott Williams assisted in the processing of the model output. Sharon Douglas of SAI assisted in the preparation of the special observations for data as-

similation, and William Neff of WPL supplied plots of the Page, Arizona, radar profiler data. Computer support was provided by CRAY Research and the National Center for Atmospheric Research, which is sponsored by the National Science Foundation. Cartographic services were provided by Matt Tharp of Deasy GeoGraphics.

REFERENCES

Anthes, R. A., E. Y. Hsie, and Y. H. Kuo, 1987: Description of the Penn State/NCAR Mesoscale Model Version 4 (MM4). NCAR Tech. Note NCAR/TN-282+STR, 66 pp. [Available from the National Center for Atmospheric Research, Box 3000, Boulder, CO, 80307.]

Barwell, B. R., and A. C. Lorenc, 1985: A study of the impact of aircraft wind observations on a large-scale analysis and numerical weather prediction system. *Quart. J. Roy. Meteor. Soc.*, **111**, 103–129.

Bell, R. S., 1986: The Meteorological Office fine-mesh data assimilation scheme. *Meteor. Mag.*, **115**, 161–177.

Errico, R. M., 1985: Spectra computed from a limited area grid. *Mon. Wea. Rev.*, **113**, 1554–1562.

Krishnamurti, T. N., H. S. Bedi, W. Heckley, and K. Ingles, 1988: Reduction of the spinup time for evaporation and precipitation in a spectral model. *Mon. Wea. Rev.*, **116**, 907–920.

Seaman, N. L., 1992: Meteorological modeling applied to regional air-quality studies using four-dimensional data assimilation. *Environmental Modeling*. P. Melli and P. Annetti, Eds., Computational Mechanics Publications, 65–88.

Stauffer, D. R., and N. L. Seaman, 1987: A real-data numerical study and four-dimensional data assimilation application for mesobeta-scale flow in complex terrain. *Proc. Symp. Mesoscale Analysis and Forecasting, Vancouver, British Columbia, Canada,* International Association of Meteorology and Atmospheric Physics (IAMAP), 533–538.

——, and ——, 1990: Use of four-dimensional data assimilation in a limited-area mesoscale model. Part I: Experiments with synoptic data. *Mon. Wea. Rev.*, **118**, 1250–1277.

——, and J.-W. Bao, 1993: Optimal determination of nudging coefficients using the adjoint equations. *Tellus*, **45A**, 358–369.

——, N. L. Seaman, and F. S. Binkowski, 1991: Use of four-dimensional data assimilation in a limited-area mesoscale model. Part II: Effects of data assimilation within the planetary boundary layer. *Mon. Wea. Rev.*, **119**, 734–754.

——, ——, T. T. Warner, and A. M. Lario, 1993: Application of an atmospheric simulation model to diagnose air-pollution transport in the Grand Canyon region of Arizona. *Chem. Eng. Commun.*, **121**, 9–25.

Zhang, D.-L., and R. A. Anthes, 1982: A high-resolution model of the planetary boundary layer—Sensitivity tests and comparisons with SESAME-79 data. *J. Appl. Meteor.*, **21**, 1594–1609.

——, H.-R. Chang, N. L. Seaman, T. T. Warner, and J. M. Fritsch, 1986: A two-way interactive nesting procedure with variable terrain resolution. *Mon. Wea. Rev.*, **114**, 1330–1339.